CMUT with mechanically coupled plate actuators for low frequencies

Marcel Krenkel[1], Michael Stolz[1], Sandro G. Koch[1] and Mario Kupnik[2]

[1] Fraunhofer IPMS, Maria-Reiche-Straße 2, 01109 Dresden, Germany
[2] Measurement and Sensor Technology, TU Darmstadt, Merckstraße 25, 64283 Darmstadt, Germany

E-mail: [1]marcel.krenkel@ipms.fraunhofer.de,
[2]kupnik@must.tu-darmstadt.de

Abstract. About 200 words

In this paper we present a structural analytical model for a capacitive micromachined ultrasonic transducer (CMUT), based on a sacrificial release fabrication process and comprised of electro-mechanical plate actuators transferring their motion to a coupling roof structure on top. The structure features a larger average displacement compared to conventional designs at lower operational frequencies.

Low operational frequencies in the range of 40 kHz to 1 MHz are beneficial for airborne applications due to their frequency-dependent strong wave attenuation in air, limiting the signal-to-noise ratio.

The eigenfrequency in dependence of the roof mass is calculated analytically and lumped elements, which can be used in equivalent circuits, are extracted. In addition, finite element analyses utilizing a shell-beam model are conducted. Experimental results, based on digital holographic microscopy, reveal the usability of the deduced model within an uncertainty of 8 %.

The developed dimensionless form of the analytical model can be used for future design purposes.

Keywords: CMUT, mechanical coupling, plate actuators, ultrasound, MEMS

Submitted to: *J. Micromech. Microeng.*

1. Introduction

Capacitive micromachined ultrasonic transducers (CMUTs), fabricated with sacrificial release technology, are limited regarding the operational frequency and the generated sound pressure. Especially for airborne applications, such as touchless gesture recognition [1], low operational frequencies between 40 kHz and 1 MHz are beneficial because the wave attenuation in air increases with increasing frequency, approximately proportional to the square of the frequency [2, 3]. Hence, a reduction of the operational frequency improves the signal-to-noise-ratio of ultrasound devices at a measurable distance.

CMUTs, presented by Haller et al. [4], have been part of active research for more than 20 years. A conventional CMUT consists of a fixed and a flexible electrode, which is deformed by an electrical excitation signal [2]. A free movement of the flexible electrode is possible, since it is located above a vacuum or gas-filled gap. An insulation layer ensures electrical separation (Fig. 1).

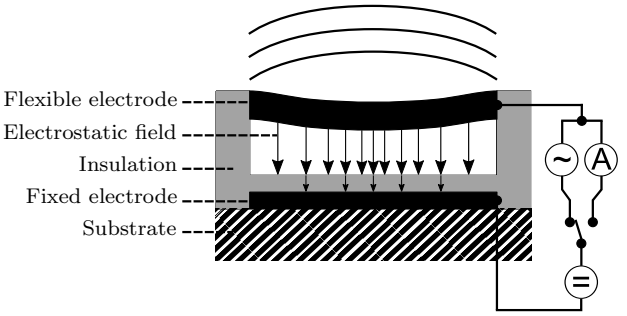

Figure 1. Conventional capacitive micromachined ultrasonic transducers (CMUTs) consist of a fixed and flexible, acoustically transmitting and receiving electrode, which is excited by the force generated in an electrostatic field. An applied DC and AC signal modulates the electrostatic field while a field change induced current is measured during reception.

The acoustic advantage of a CMUT is its good impedance matching without matching layers, especially to water [5]. The positive implication is a broadband transducer, allowing short acoustic pulses, resulting in improved image resolution. As MEMS device, advantages of microtechnologies are inherently present in CMUTs [6]. Scalibility as well as CMOS compatibility are only two well known advantages, increasing the reliability and the ease of use due to integrated signal generation and processing [6].

Regarding the disadvantages, devices fabricated with sacrificial release technology have a limited frequency range and restricted sound pressure. Larger plate actuators for lower frequencies, required in airborne applications, are not feasible due to stress related issues.

Furthermore, CMUT plates are electrically connected in parallel to achieve larger sound pressure and to form a larger acoustic aperture [Fig. 2(a)]. Remaining non-active areas do no contribute to acoustic radiation and receiving performance. Moreover the vibrating plates have a specific deflection shape [7], which additionally limits the radiated sound pressure.

Mechanically coupled actuators, discussed in this paper, are already a common approach in the application field of adaptive optics. Spatial light modulators are used here to correct aberrations of optical systems [8] by adjustments of the phase of an incoming wave. A common approach for those light modulators are membrane deformable mirrors (MDM) [8, 9], also fabricated as MEMS devices [10, 11]. These structures comprise a continuous mirror surface and underlying actuator units, which are capable to deform the mirror. Such systems avoid undesired diffraction and benefit from a better phase manipulation. The mechanical coupling of the actuators allows a smooth deformation of the mirror surface while exciting several actuators to enable a reflection without scattering [9, 11]. For ultrasound devices however, a piston-like motion is desired to increase the overall deflection.

The simulation of several coupled actuators and the fabrication of such free-standing structures are challenging. Multiphysical simulations are extensively performed with finite element methods (FEM) for CMUTs [5]. This approach is especially beneficial in order to calculate parameters of complex geometries or to investigate the interactions between physical domains in detail. In case of mechanically coupled systems, this modelling approach requires extensive computational power due to the size of a model.

Hence, analytical models provide a fast insight into parameter dependencies and can estimate crucial parameter, such as the eigenfrequency of a system. For the mechanically coupled actuators, the distribution of the mass needs to be regarded as it has a significant impact on the system behavior.

This paper presents a CMUT with mechanically coupled plate actuators and its analytical modeling. The model is validated by FEM simulations of

an exemplary structure and experimental motion measurements.

The structure is organized as follows: Section two outlines the idea of the MEMS structure. The analytical model with the underlying assumptions, the definition of the mathematical model and the solution approach for the mechanically coupled structure is deduced in the third section. Section four covers the verification of the analytical model by means of FEM calculations. Experimental investigations in comparison to the simulations are presented in section five, focusing on the displacement of the structure. Finally, conclusions are drawn and future research activities are outlined.

2. Mechanically coupled CMUT concept

Our approach of mechanically coupled actuators in CMUTs is inspired by the MEMS mirror technology, which uses large flat moving plates. Our CMUT plates [Fig. 2(a)], acting as electro-mechanical drive, are coupled via pillars and a roof structure on top [Fig. 2(b)]. Note that in this configuration the large maximum deflection in the center of a plate actuator is transferred to the roof structure. Similar concepts were contrived by Huang [12], but a thorough design and analysis of such CMUT structures are not known to be published yet.

As one can easily observe, the acoustically radiating surface is separated from the electro-mechanical transforming geometry. The thereby gained design freedom enables new designs for the electro-mechanical actuator, such as spring-mass structures that are commonly used for acceleration sensors and other MEMS devices.

A piston-like motion of the roof structure is desired, which increases the fill factor of the device and thereby the output pressure [**?**]. In addition the large active area performs as large pressure receiver, transforming the incoming pressure into a large mechanical force for the transduction actuators.

The additional roof mass increases the mass of the entire system, and, thus, reduces its eigenfrequency. While the roof mass adjusts the eigenfrequency, the lateral dimensions of the plate actuators are kept as small as possible to reduce the stress sensitivity of the plates.

3. Analytical model for rigidly coupled systems

3.1. Model assumptions and desciption

The advantages of an analytical model are a faster simulation and insight in physical relationships, which are not easily recognizable by experiments or time consuming FEM simulations. Furthermore, a fast parameter simulation estimates a plausible parameter space for numerical calculations and serves as validation of more complex calculations. The herein derived model also can be used to develop a multiphyics model with lumped parameters according to Wygant et al [7]. The basis of the presented model is the mathematical description of P. A. A. Laura et al [13].

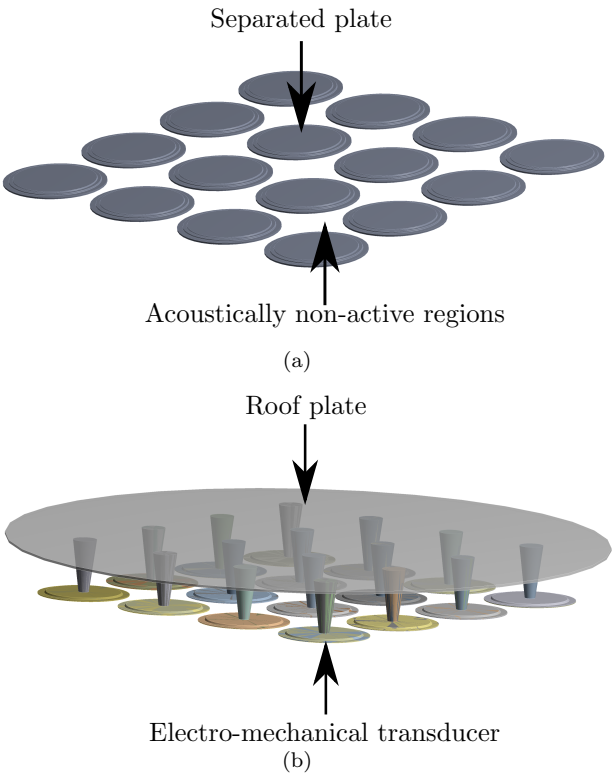

Figure 2. a) Conventional CMUT of separated plates and b) CMUT with mechanically coupled plate actuators. Electrostatic excited motion of plate actuators is transferred to a roof plate via the center pillars.

Sufficient and plausible model assumptions, which are assumed to describe the physical behavior, are:

(i) A uniform motion of the roof plate;
(ii) Local stiffening due to the roof pillar attached to the bottom plate actuator is neglected;
(iii) The actuator is a thin circular plate [14];
(iv) An isotropic material is used;
(v) Fixed clamping of the plate actuator.

The assumption (i) is deduced from the desire to build a piston radiator emitting large sound pressure waves. The roof plate can be modeled as additional point mass m_c (Fig. 3).

Assumption (ii) is valid, if the radius of the pillar is significantly smaller than the plate radius. The flexural rigidity of a conventional plate approximates the stiffness of the pillar-coupled structure. In our

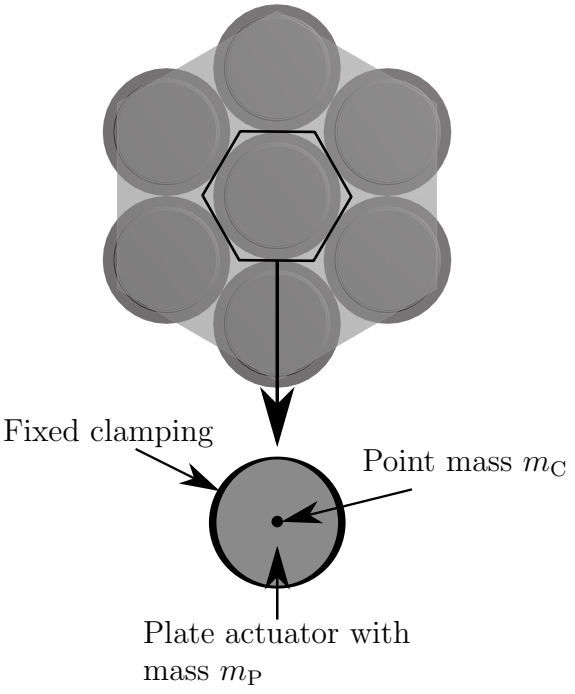

Figure 3. Approximation of a mechanically coupled structure with uniform roof plate motion as clamped circular plate, holding a geometrical mass m_P, with point mass m_C in the center.

chosen designs the ratio between pillar radius and the plate radius is only 4 %.

A circular plate actuator [assumption (iii)] has a significantly larger bending stiffness than in-plane stretching stiffness of a pure membrane [14]. Nonlinear effects such as stress stiffening [15] are neglected in this model for convenience.

The material of the oscillating system is assumed to be isotropic [assumption (iv)], which is valid due to the used amorphous plate material [16, 17].

Fixed clamping [assumption (v)] is modelled with zero deflection, i.e.

$$w(r = a) = 0 \tag{1}$$

and no structural rotation

$$\left.\frac{dw(r)}{dr}\right|_{r=a} = 0 \tag{2}$$

at the boundary $r = a$ of the plate with radius a depending on the technological design [18].

The time-harmonic partial differential equation, describing the behavior of the system, is

$$\underbrace{D\nabla^4 w(\boldsymbol{r})}_{\text{Flexural force}} - \underbrace{\rho h\omega_0^2 w(\boldsymbol{r})}_{\substack{\text{Inertial force}\\ \text{of the plate}}} - \underbrace{m_C\omega_0^2\delta(\boldsymbol{r})w(\boldsymbol{r})}_{\substack{\text{Inertial force}\\ \text{of the point mass}}} = 0 \tag{3}$$

with the flexural rigidity D, mass density ρ and the thickness h of the plate actuator. This equation is exactly the same in classical thin plate theory [19] except the last term that represents the effect of the point mass m_C in the center of the plate [13].

A solution is searched for the deflection $w(\boldsymbol{r})$ and the eigenfrequenz $\omega_0 = 2\pi f_0$ of the axisymmetric deformation of the plate. Therefore equation (3) can be written in cylindrical coordinates

$$\nabla^4 w(\bar{r}) - \Omega^2 w(\bar{r}) - \Omega^2 r_{\text{mass}}\frac{\pi}{\bar{r}}\delta(\bar{r})w(\bar{r}) = 0, \tag{4}$$

neglecting the angular coordinate due to the axisymmetric assumption. Furthermore, the radial coordinate r is transformed into a dimensionless form $\bar{r} = \frac{r}{a}$. The eigenvalue

$$\Omega^2 = \omega_0^2\frac{\rho h}{D}a^4 \tag{5}$$

can be used to calculate the eigenfrequency by means of the material parameters ρ, D and the geometrical parameters h, a. If these parameters are unknown, the relation

$$\frac{\Omega_C}{\omega_C} = \frac{\Omega_P}{\omega_P}, \tag{6}$$

with the eigenvalue Ω_P and eigenfrequency ω_P of the uncoupled system can be used to calculate the eigenfrequency ω_C of the coupled system with a roof mass. Then the eigenvalue Ω_C of the coupled system for a specific mass ratio

$$r_{\text{mass}} = \frac{m_C}{m_P} \tag{7}$$

between the point mass m_C and the geometrical mass $m_P = \pi a^2 h\rho$ has to be determined by solving equation (4).

3.2. Model solution

According to Laura et al [13], the Galerkin method is used as solution approach. Hence a trial function

$$w(\bar{r}, c) = A\left(\frac{2}{c-2}\bar{r}^{\,c} - \frac{c}{c-2}\bar{r}^{\,2} + 1\right), \tag{8}$$

with the optimization parameter c and the amplitude A is defined to calculate the best-fit solution for the differential equation (4).

The Galerkin method yields an approximate solution, which is the projection of the exact, unknown solution into the subspace of trial functions. Therefore the integral

$$G(c, A) = \int_S w(\bar{r})R(w(\bar{r}))dS = 0 \tag{9}$$

has to be solved, which represents the scalar product between the trial functions and a residuum $R(w(\bar{r}))$. The residuum is the equilibrium error that results by inserting the trial function $w(\bar{r})$ into the differential equation (4).

If the trial function $w(\bar{r})$ and the residuum $R(w(\bar{r}))$ are inserted into the functional $G(c, A)$, the general optimization function

$$\Omega^2(c) = \frac{\int_0^1 w(\bar{r}, c)\nabla^4 w(\bar{r}, c)\bar{r}d\bar{r}}{\int_0^1 w^2(\bar{r}, c)\bar{r}dr + \frac{r_{\text{mass}}}{2} w^2(\bar{r} = 0, c)} \tag{10}$$

is found for an arbitrary trial function and mass ratio r_{mass}. An evaluation of this expression reveals

$$\Omega^2(c) = \frac{12c^2}{(c-1)\left(\frac{c^2(5+c)}{(1+c)(2+c)(4+c)} + 3r_{\text{mass}}\right)} \tag{11}$$

for optimization parameters $c > 2$. Otherwise the trial function $\tilde{w}(\bar{r}, c = 2)$ is not defined for real values. An eigenvalue for a specific c is an upper bound to the true eigenvalue according to Rayleigh's principle [14]. Therefore a minimized error $G(c, A)$ with corresponding eigenvalue Ω is obtained by numerically minimizing the eigenvalue function (11) as function of the parameter c.

3.3. Eigenfrequency reduction, bending shape and lumped elements

Model results will be presented as non-dimensional parameters, which enable the flexible calculation of dimensional values for a specific system with varying material and geometrical parameters. Dimensionless lumped elements are extracted from the derived deflection shapes.

The eigenvalue of the roof coupled system reduces drastically with increasing mass ratio (Fig. 4). Thereby the additional roof mass allows to adjust the eigenfrequency, while the actuator parameters are kept constant. As described by the Rayleigh principle, the approximate eigenvalue of the conventional plate ($r_{\text{mass}} = 0$) is with a value of 10.2261 only 0.1 % larger than the exact eigenvalue of 10.2158 [19]. The deviation between these two values is a result of the minimization problem.

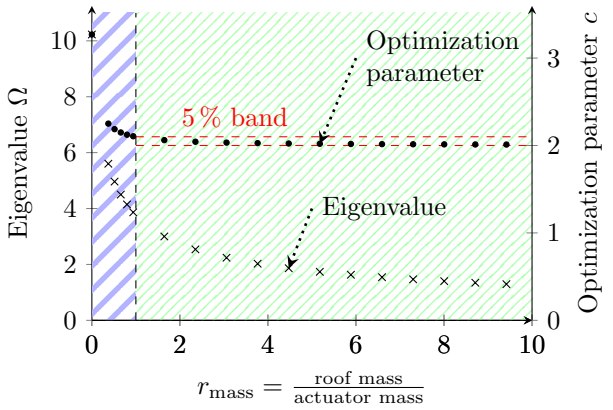

Figure 4. Descending non-dimensional eigenfrequency and optimization parameter in dependence of the mass ratio.

The eigenvalue and optimization parameter functions in dependence of the mass ratio can be separated into a region with a large and with a small change of the optimization parameter (Fig. 4). The optimization parameter converges to the value $c \to 2$. At the chosen limit $r_{\text{mass}} = 1$, the optimization parameter does not deviate by more than 5 % from the convergence limit. In case of large mass ratios, the eigenvalue and the eigenfrequency decrease linearly with the mass ratio.

The behavior of the optimization parameter is connected to the deflection shapes of the actuator (Fig. 5). The descending slope of the frequency reduction curve is reflected by the deflection shapes of the actuator. In the blue region ($r_{\text{mass}} < 1$), the deflection shape of the plate actuator changes significantly compared to the deflection shape of a conventional actuator without point mass. The deflection shape exhibits only small changes for large mass ratios ($r_{\text{mass}} > 1$) in the green region.

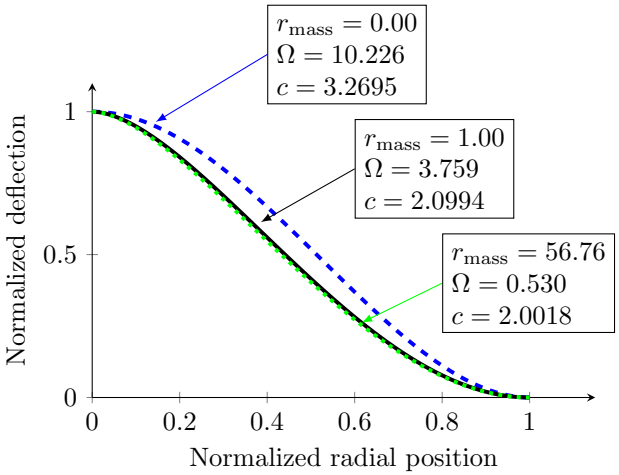

Figure 5. Deflection shape functions for different mass ratios. As the mass ratio increases, the deflection shapes changes significantly up to $r_{\text{mass}} = 1$.

A similar behavior can be recognized in the lumped elements, which can be extracted from the deflection shapes of the actuator. The effective, lumped mass of the actuator plate can be calculated with an energy approach. The kinetic energy

$$E_{\text{k}} = \frac{1}{2}\int_0^1 2\pi\rho h[\omega_0 w(\bar{r})]^2 \bar{r}d\bar{r} = \frac{1}{2} m_{\text{eff}}(\omega_0 w_{\text{eff}})^2 \tag{12}$$

of the distributed actuator mass equals a virtual, effective mass m_{eff} with one effective degree of freedom w_{eff} [7]. After rearrangement the effective, lumped mass is calculated by

$$m_{\text{eff}} = 2\pi\rho h \int_0^1 \left[\frac{w_{\text{pk}}}{w_{\text{eff}}} w(\bar{r})\right]^2 \bar{r}d\bar{r} \tag{13}$$

at the eigenfrequency ω_0.

The choice of the effective deflection w_{eff} depends on the energy flow between different energy storages in the system. An appropriate choice is $w_{\mathrm{eff}} = w_{\mathrm{pk}}$ because the maximum deflection of the actuator is transferred to the roof mass via the pillars in the center of the actuator, i.e. the kinetic energy of the roof mass depends on the center deflection.

Thus, the effective mass of the actuator can be used to calculate the effective stiffness

$$k_{\mathrm{eff}} = \omega_0^2 (m_{\mathrm{eff}} + m_{\mathrm{C}}), \tag{14}$$

with the eigenfrequency ω_0, calculated with the approximate solution of the eigenvalue (5), (6).

A non-dimensional, relative effective mass

$$r_{\mathrm{m,eff}} = \frac{m_{\mathrm{eff}}}{m_{\mathrm{p}}} \tag{15}$$

is defined because of the scalability of this expression and because of the very small mass values which are typical for microstructures.

Furthermore, a non-dimensional, relative, effective stiffness

$$r_{\mathrm{k,eff}} = \frac{k_{\mathrm{eff}} a^2}{\pi D} = \Omega^2 (r_{\mathrm{m,eff}} + r_{\mathrm{mass}}) \tag{16}$$

is defined, which can be calculated with the other non-dimensional parameters Ω, r_{mass} and $r_{\mathrm{m,eff}}$.

The effective mass (Fig. 6) and the effective stiffness (Fig. 7) decrease strongly due to a small mass ratio r_{mass} change at small mass ratios.

These relative effective parameters decrease similarly as the optimization parameter, which determines the deflection shapes. For large mass ratios, the relative effective parameters converge to constant limits.

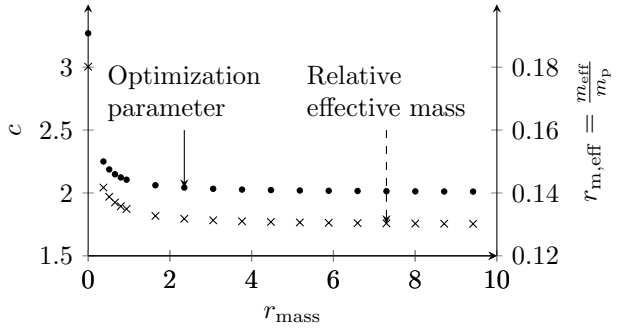

Figure 6. Effective mass ratio of the actuator and optimization value in dependence of the mass ratio reduces similarly.

The inspection of the eigenvalue

$$\Omega^2 = \frac{r_{\mathrm{k,eff}}}{r_{\mathrm{m,eff}} + r_{\mathrm{mass}}}, \tag{17}$$

deduced from equation (16), highlights the dependence of the eigenfrequency on the relative parameters. Two reasons for the frequency reduction can be found.

First, a significant reduction of the eigenfrequency occurs due to the change of the mass distribution of the actuator and the related change of the deflection shape (Fig. 5). In this transition region ($0 < r_{\mathrm{mass}} < 1$), a stronger reduction of the eigenvalue and, thus, of the eigenfrequency can be achieved because the decreasing relative effective parameters are also functions of the mass ratio.

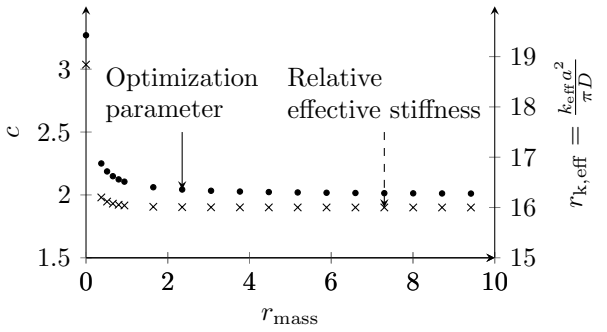

Figure 7. Effective stiffness ratio of the actuator reduces similarly to the effective mass (Fig. 6).

Second, the center mass dominates the behavior of the actuation structure for large mass ratios ($r_{\mathrm{mass}} \geq 1$). As described, the relative effective parameters $r_{\mathrm{k,eff}}$ and $r_{\mathrm{m,eff}}$ can be assumed constant for large mass ratios $r_{\mathrm{mass}} > 1$ (Fig. 6, 7). The eigenvalue only depends approximately on the mass ratio

$$\Omega^2 \approx \frac{16}{0.13 + r_{\mathrm{mass}}}, \tag{18}$$

while the relative effective parameters become independent of the mass ratio. For the system design an additional parameter, i.e. the mass ratio r_{mass}, can be utilized to define the eigenfrequency in addition to the radius a and the thickness h of the actuator for a specific material system.

The dimensionless relative parameters herein derived can be used to specify a system arbitrarily, consisting of a plate with a mass acting in the center of the plate, for a specific eigenfrequency. The model takes into account the effect of the center mass on the effective parameters.

3.4. Comparison with exact bending shapes

The comparison with exact analytical bending shapes validates the so far deduced model for the theoretical limits and underlines the observed changes of the bending shapes due to the center mass. In case of $c = 4$ the trial function is equivalent to the static deflection shape

$$w(\bar{r}) = A\left(1 - 2\bar{r}^2 + \bar{r}^4\right) = A\left(1 - \bar{r}^2\right)^2 \tag{19}$$

of a uniformly loaded circular plate [20]. However, for a conventional plate without center mass ($r_{\mathrm{mass}} = 0$), an optimization parameter of $c = 3.2695$ is obtained.

Then the trial function approximates the exact dynamic deflection shape

$$w_{\mathrm{dyn}}(\bar{r}) = J_0\left(3.197\bar{r}\right) - \frac{J_0(3.197)}{I_0(3.197)} I_0\left(3.197\bar{r}\right) \tag{20}$$

of the fundamental mode of a conventional plate [14, 21] with the Bessel function J_0 and modified Bessel function I_0 of the first kind.

Using w_{pk} as effective coordinate results in an exact relative effective mass of 0.2 with the static deflection shape [7], while the Galerkin method yields 0.1802. Then the relative effective stiffness of the exact solution is 20.87, while the approximate value amounts to 18.84.

The effect of the roof mass ($r_{\mathrm{mass}} > 0$) can be interpreted as inertial force acting in the center of the plate actuator. The deflection shape

$$w(r) = \frac{Fr^2}{8\pi D} \ln\left(\frac{r}{a}\right) + \frac{F}{16\pi D}(a^2 - r^2) \tag{21}$$

describes this load case with the center force F [20]. An extreme value determination in conjunction with a limit value calculation at $r \to 0$ is utilized to determine the maximum amplitude

$$w_{\mathrm{pk}} = \frac{Fa^2}{16\pi D} \tag{22}$$

of equation (21). Then the non-dimensional equation

$$\frac{w(\bar{r})}{w_{\mathrm{pk}}} = \left(2\bar{r}^2 \ln\left(\bar{r}\right) - \bar{r}^2 + 1\right), \tag{23}$$

with the dimensionless spatial coordinate $\bar{r} = r/a$ can be compared with the trial functions.

According to the approach (13), an effective mass of $m_{\mathrm{eff}} = (7/54)\ m_{\mathrm{P}}$ can be calculated with the deflection shape (23). For large mass ratios, the relative effective mass converges to this theoretical value $7/54 = 0.129\,63$ (Fig. 6).

The relative effective stiffness is determined according to equation (16) with an eigenvalue of 0.336 at a large mass ratio of 141.54. The resulting relative effective stiffness is 15.999 (Fig. 7).

As the effective parameters of the actuator change, the electrical excitation of the system is influenced as well. Keeping in mind, that assumption (ii) is considered valid, the static stiffness is approximated by the stiffness of a conventional plate. In the dynamic case the stiffness is significantly lower because of the influence of the roof mass. Whereas the static and dynamic stiffness of a conventional CMUT are similar [7].

The larger static stiffness increases the required DC voltage which is beneficial for the electro-mechanical transformation factor [22] and the resulting receive sensitivity. Nevertheless, the effort to design a circuit for DC generation, especially in mobile devices, can be more challenging. As opposed to this, it is presumed that a lower AC signal is necessary to excite the structure or larger deflections can be achieved with the same AC voltage compared to a conventional CMUT. Further research efforts will be needed to verify this presumption.

Furthermore the extracted lumped elements can be included into an equivalent circuit, enabling the simulation of transmit and receive sensitivity as well as the combined design of transmit and receive electronics. According to the piston-like roof motion, the acoustic impedance can be modelled by a piston impedance [23].

4. Structural mechanical finite element model

4.1. Model description

A finite element model of a CMUT with mechanically coupled actuators was developed in ANSYS Workbench 17.2 to investigate the structural, dynamic behavior and to verify the assumptions of the analytical model.

Analyses of the structural eigenvalue problem were conducted to observe the influence of the pillar and roof structure on the oscillation mode and the eigenfrequency. The model is based on structures which are currently in fabrication.

The model, consisting of seven coupled plate actuators (Fig. 8), is developed with shell elements for the actuators and roof plate and beam elements for the pillar structures. The overlap Δa, which is the boundary of the roof plate at the outer actuators, can be used to optimize the dynamic roof deformation [21].

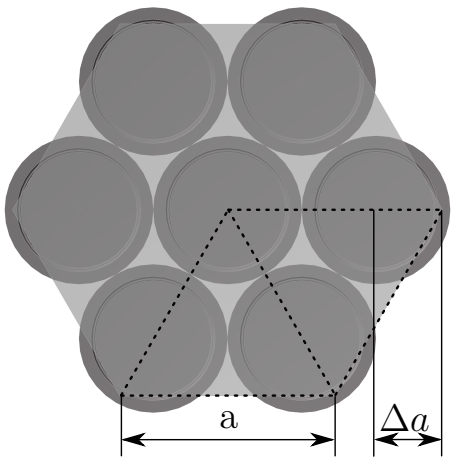

Figure 8. FEM description of seven coupled actuators with the size a of the hexagonal roof and the overlap Δa of the roof at the last actuator pillars.

The verification of the shell-beam model is done by comparing this model with a solid model for different

roof overlaps and layer ratios, i.e.

$$r_{\text{layer}} = \frac{\text{roof thickness}}{\text{actuator thickness}}, \tag{24}$$

which is the roof to actuator thickness ratio. The resulting relative deviation between the eigenfrequencies of the solid and shell-beam model is approximately 3 % in the investigated parameter range, which verifies the validitiy of this FEM model to investigate the system behavior. The structures are investigated with a fixed pitch between the plate actuators.

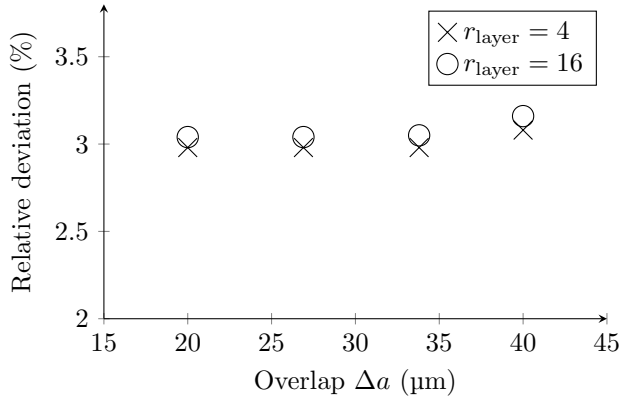

Figure 9. Comparing the deviations of eigenfrequencies of the solid model with the shell-beam model.

4.2. Mechanically Coupling of Actuators

Two different coupling cases can be distinguished by analyzing the structural eigenvalue problem (Fig. 10). The most desired case is a rigid coupling, which exhibits a uniform piston-like roof plate motion. The roof plate can be described as distributed mass. Higher modes, such as tilting of the roof plate, are also existent due to the distribution of the roof mass and strongly depend on the geometry. Such an approximately rigidly coupled system can be realized by a large layer ratio between roof stiffness and actuator stiffness. The choice of a stiffer roof material as well as a thicker roof plate in order to increase the roof stiffness is limited by the used technology.

If the stiffness of the roof plate is not large enough compared to the actuator stiffness, the roof structure deforms elastically and exhibits spring behavior. A roof with a stiffness in the range of the actuator stiffnes will manifests global modes with several radial or angular oscillations (Fig. 11). Higher modes with zero-crossings in their spatial oscillation (Fig. 11) do not contribute to radiation with the zero amplitude regions but limit the usable frequency range if such modes are close to desired resonances. All actuators oscillate with a diverging phase and the excitation of sound waves cannot be modeled with the piston model.

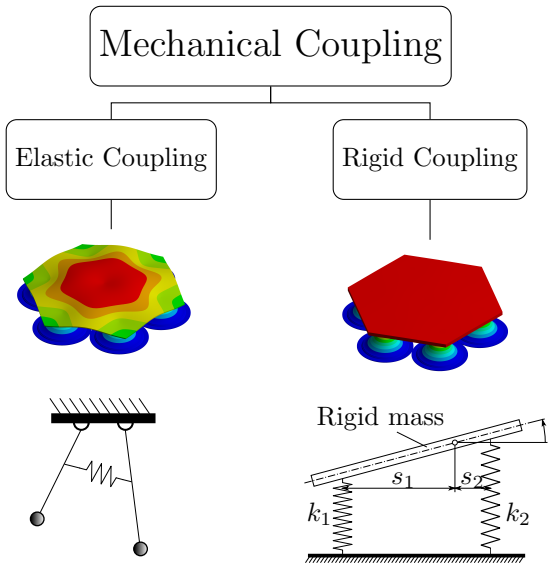

Figure 10. Classification of mechanical coupling as comparison of a simple two oscillator systems with a multiple degree CMUT structure [24].

If the roof thickness becomes smaller than the actuator thickness, the actuators and pillars will only deform the roof locally with a small mechanical coupling between the actuators [9]. This type of coupling can reduce the eigenfrequency of the system due to the additional mass but lacks the desired high overall deflection.

Furthermore the stiffness of the roof plate depends not only on the thickness and material choice but also on the lateral size of the plate. For instance, the spring constant of a circular plate, i.e.

$$k_1 = \frac{16\pi E}{(1-\nu^2)} \frac{t_{\text{act}}^3}{r_{\text{act}}}, \tag{25}$$

depends also on the radius r_{act} beside the Young's modulus E, Poisson's ratio ν and the plate thickness t_{act} [25].

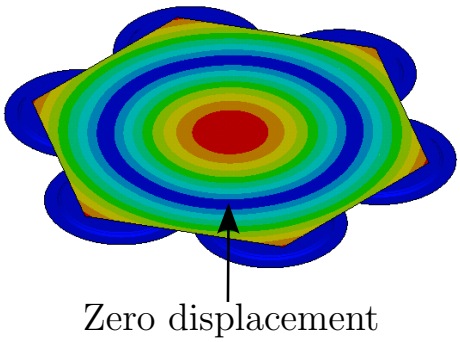

Figure 11. Higher mode of seven coupled actuators with zero-crossings in the deflection shape (layer ratio = 4) as indicated by blue color.

Elastically coupled system can still exhibit a uniform roof motion if an optimization of the overlap is conducted [21]. The eigenfrequency of a seven actuator system with the most uniform roof plate motion, calculated by FEM analysis, is 525.7 kHz. The result of the analytical model with the same parameter configuration is 509.2 kHz, i.e. a relative deviation of only 3.2 %.

5. Measurement of the roof motion

Beside optimized structures, which are currently in fabrication, preliminary test structures with prefabricated actuators are used to fast-track the experimental investigations. The herein investigated MEMS devices exhibiting a rectangular aperture and a layer ratio $r_{\text{layer}} = 1$ contain 90 electrostatically excited circular plates in a hexagonal pattern. This roof coupled structure is compared with a reference structure comprised of the same 90 actuators without pillars and a roof structure.

Electrical impedance measurements already show a reduction of the resonance frequency [21], but do not verify the motion of the roof plate. The herein presented static and dynamic motion data was measured with a digital holographic microscope (LynceeTec, R-Series, Switzerland) to verify the theoretical predictions of the analytical model and FEM. Displacement patterns are investigated by sweeping the excitation frequency in time. The surface averaged displacements and the corresponding resonance frequency are deduced from this data.

As expected for an electrostatic system, the static, surface-averaged deflection $\bar{w}$ in dependence of a DC voltage exhibits a nonlinear curve (Fig. 12) [26]. Furthermore, the coupled roof structure has a larger deflection at the same DC voltage compared to the uncoupled reference structure. The increased

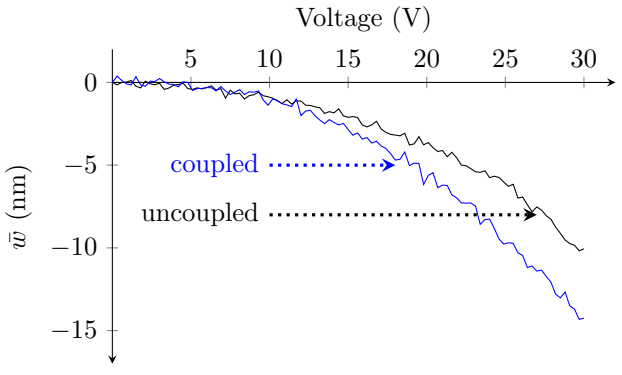

Figure 12. The surface averaged, static deflection of an uncoupled, conventional CMUT and a mechanically coupled CMUT, showing a larger deflection of a roof coupled structure at the same DC voltage.

deflection is achieved by avoiding position dependent deflection shapes (Fig. 5), as well as non-moving areas between the plates due to the large roof plate with a large fill factor.

According to the analytical model, the eigenfrequency of the reference device is estimated at $f_0 = 5.57$ MHz. The eigenvalue of the roof structure is calculated to 3.99 at a mass ratio of 0.87 by means of the derived analytical model. Then an eigenfrequency of 2.18 MHz yields with the help of the eigenvalue ratio [equation (6)].

The dynamic measurements of the surface averaged deflection with the same excitation voltages for both reference and roof coupled structure reveal a significant resonance reduction (Fig. 13). While the reference structure shows a significant resonance at $f_r = 6.88$ MHz, the coupled structure has a reduced resonance at $f_r = 2.58$ MHz. Thereby the resonant frequency of the reference structure is higher than the estimated eigenfrequency of a circular plate (18 % deviation). Possible reasons, which are not modeled analytically, are tensile material stress due to fabrication as well as stress generated by the predeflection of the plate due to ambient pressure [27, 28, 29].

The eigenfrequency of the coupled system deviates by 15.5 % from the analytical model which does not predict the reference eigenfrequency correctly. If the measured resonant frequency of the reference actuator is taken into account [equation (6)], the eigenfrequency of the roof structure will result in 2.66 MHz and estimates the measured frequency with 8 % uncertainty.

In contrast to the static deflection results, the resonant deflection $\bar{w}_r$ of the roof coupled structure is smaller than the surface averaged deflection of the uncoupled reference due to the uneven deformation of the roof plate. Possible explanations are the soft coupling due to a small layer ratio r_{layer} between the roof plate and actuators as well as an asynchronous motion [Fig. 14(a)] of the actuators which is transferred to the roof. The out-of-phase displacement of different roof structure positions reduces the average of the entire roof surface [Fig. 14(b)].

A further evidence of the electrostatic behavior is the increasing resonance amplitude in dependence of an increasing DC voltage (Fig. 15). A shift of the resonance frequency due to electrostatic softening [22] is not observed in the measured data. The pull-in is measured to be about 50 V, so that the used DC voltages correspond to only 20 %, 33 % and 50 % of this pull-in estimation, respectively. This means that the spring softening effect is too weak to be visible in the data. These voltages were chosen to prevent the destruction of these preliminary structures due to large oscillation amplitudes in air.

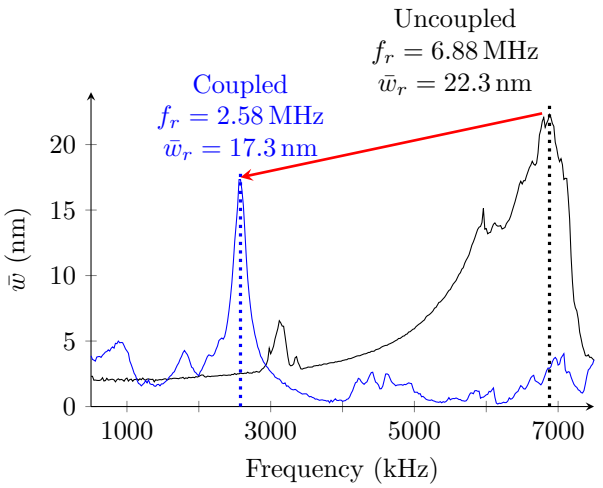

Figure 13. Surface averaged frequency response of a conventional CMUT as reference and a CMUT with roof coupled actuators. The same DC and AC voltages were used to excite the devices. A significant resonance of the coupled structure below the resonance of the reference structure can be observed.

The measured frequency responses of the displacements verify the electrostatic behavior of the structures and a reduced resonance frequency due to a roof structure. However, the desired piston-like motion of the roof structure cannot be observed. Out-of-phase displacements at different positions of the investigated devices are present. In particular the boundary of the roof plate exhibits a larger displacement than the inner areas, indicating a soft roof plate due to the low layer ratio. The devices fabricated currently are optimized with a larger layer ratio in order to stiffen the roof structure. Further insight into the acoustic performance of the investigated devices cannot be obtained due to the complex deformation without acoustic simulation or acoustic measurements.

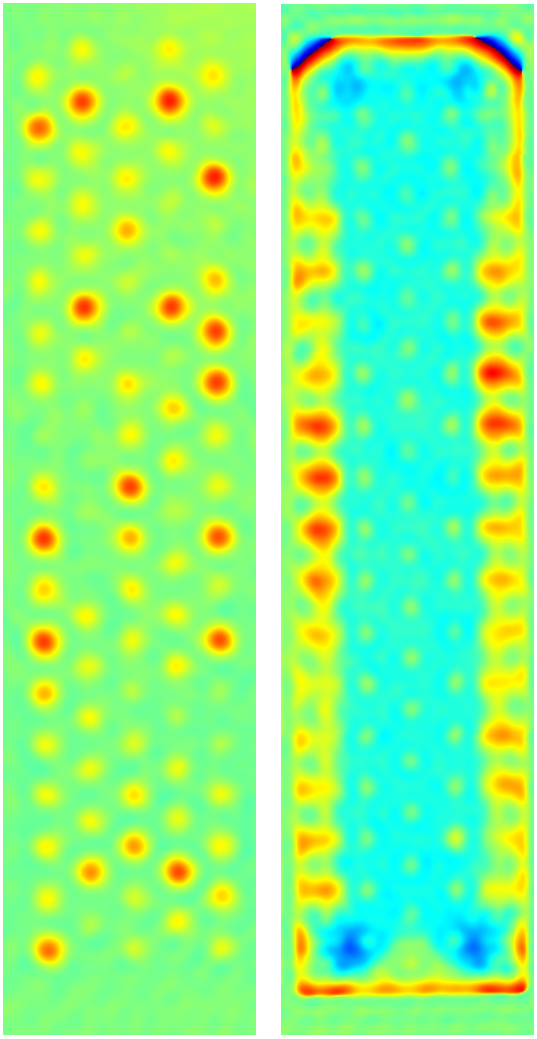

Figure 14. Normalized mode shapes of the highlighted resonances in Fig. 13 of a) the reference structure and b) the roof coupled structure. The illustrated shapes are extracted at the time of the maximum surface averaged displacement.

6. Conclusion

A CMUT approach comprised of electro-mechanical plate actuators coupled via a pillar-roof structure was presented along with a structural analytical model to estimate the eigenfrequency of the system in dependence of the roof mass and the plate actuator parameters. The deduced dimensionless model permits system designers to specify geometrical parameters for a defined eigenfrequency with an additional degree of freedom, i.e. the roof mass.

Finite element analyses revealed that the roof coupling affects the eigenfrequency and the mode shape that can deviate from the desired piston-like motion.

The measured results prove the feasibility of these coupled structures with CMOS compatible sacrificial release technology as well as a frequency reduction in accordance with the theoretical results. If the resonance frequency of the pure actuators is known, an uncertainty of 8 % between analytical eigenfrequency and measured resonance frequency of the roof coupled structure is observed. Dynamic measurements revealed, that a piston-like motion could not be obtained in accordance with the analytical assumption in the investigated frequency range. An optimized design with a thicker layer ratio is currently in fabrication in order to achieve a more homogenous motion.

Future work will include the characterization of structures with the improved fabrication process. Acoustic measurements are required to verify acoustic presumptions based on the measured displacement results.

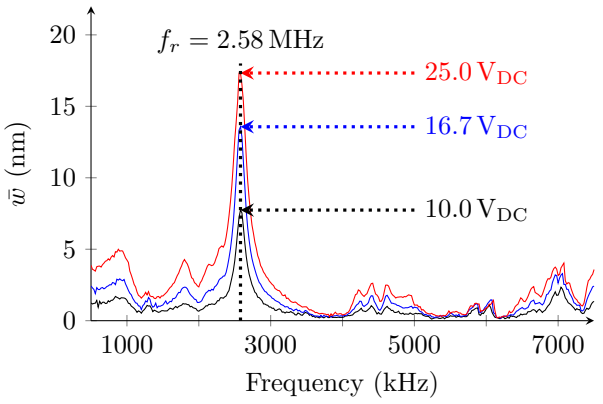

Figure 15. Surface averaged frequency responses of a roof coupled structure exhibit a DC voltage dependent resonance amplitude at $f_r = 2.58\,\mathrm{MHz}$ as a result of an increasing electro-mechanical transformation factor. A voltage dependent reduction of the resonance frequency as effect of electrostatic softening is not observable.

With regard to modeling, the description of the system with an equivalent circuit, including the electrostatic transduction and the acoustic radiation, can provide more insight into the electrical behavior, beneficial for the design of transmit and receive electronics.

Acknowledgments

This research was partially funded by an internal project of the Fraunhofer society (project number: 832 308). Parts of this work were done in the ECSEL project "Advanced Distributed Pilot Line for More-than-Moore Technologies" (ADMONT) under the grant agreement No 661796. The authors thank all involved Fraunhofer colleagues for their support, especially from the departments environmental sensing and engineering at Fraunhofer IPMS.

References

[1] T. Dahl, J. L. Ealo, H. J. Bang, S. Holm, and B. T. Khuri-Yakub. Applications of airborne ultrasound in human-computer interaction. *Ultrasonics*, 54(7):1912–1921, 2014.

[2] M. I. Haller and B. T. Khuri-Yakub. A surface micromachined electrostatic ultrasonic air transducer. *IEEE Transactions on Ultrasonics, Ferroelectrics and Frequency Control*, 43(1):1–6, 1996.

[3] F. Massa. Ultrasonic transducer for use in air. In *Proceedings of the IEEE*, volume 53, pages 1363–1371, 1965.

[4] M. I. Haller and B. T. Khuri-Yakub. A surface micromachined electrostatic ultrasonic air transducer. In *IEEE Ultrasonics Symposium*, 1994.

[5] A. S. Ergun, G. G. Yaralioglu, O. Oralkan, and B. T. Khuri-Yakub. Techniques and applications of capacitive micromachined ultrasonic transducers. In Cornelius T. Leondes, editor, *MEMS NEMS Handbook Techniques and Applications*, pages 223–285. Springer Science + Business Media, Inc., 2005.

[6] A. D. Romig, M. T. Dugger, and P. J. McWhorter. Materials issues in microelectromechanical devices: science, engineering, manufacturability and reliability. *Acta Materialia*, 51(19):5837–5866, 2003.

[7] I. O. Wygant, M. Kupnik, and B. T. Khuri-Yakub. An Analytical Model for Capacitive Pressure Transducers With Circular Geometry. *IEEE Journal of Microelectromechanical Systems*, 27(3):448–456, 2018.

[8] P. M. Birch, R. Young, and C. Chatwin. Spatial Light Modulators (SLMs). In Gabriel Cristobal, Peter Schelkens, and Hugo Thienpont, editors, *Optical and Digital Image Processing: Fundamentals and Applications*. Wiley-VCH, 2011.

[9] R. K. Tyson. *Introduction to Adaptive Optics*. SPIE Press, Bellingham, Waschington, 2000.

[10] T. G. Bifano, J. Perreault, R. Krishnamoorthy Mali, and M. N. Horenstein. Microelectromechanical deformable mirrors. *IEEE Journal of Selected Topics in Quantum Electronics*, 5(1):83–89, 1999.

[11] S. A. Cornelissen, A. L. Hartzell, J. B. Stewart, T. G. Bifano, and P. A. Bierden. MEMS deformable mirrors for astronomical adaptive optics. In *Proc. SPIE 7736, Adaptive Optics Systems II*, volume 77362D. 2010.

[12] Y. Huang. Micro-electro-mechanical transducer having a surface plate. Number US 8018301 B2, 2011.

[13] P. A. A. Laura, P. A. Laura, G. Diez, and V. H. Cortinez. A note on vibrating circular plates carrying concentrated masses. *Mechanics Research Communications*, 11(6):397–400, 1984.

[14] A. W. Leissa and M. S. Qatu. *Vibrations of Continuous Systems*. McGraw-Hill, 2011.

[15] M. Kupnik, I. O. Wygant, and B. T. Khuri-Yakub. Finite element analysis of stress stiffening effects in cmuts. In *IEEE Ultrasonics Symposium*, 2008.

[16] J. Schmidt, M. Friedrichs, and A. Gehner. Amorphous TiAl films for micromirror arrays with stable deflection integrated on complementary metal oxide semiconductors. *Journal of Micro/Nanolithography, MEMS, and MOEMS*, 7(2), 2008.

[17] M. Krenkel, N. Lange, S. G. Koch, and M. Kircher. Mechanically coupled capacitive ultrasonic transducer. In *Smart System Integration*, 2018.

[18] L. Elsaesser, M. Friedrichs, M. Klemm, and A. Unamuno. Stress controlled CMUT fabrication based on a CMOS compatible sacrificial release process. In *Symposium on Design, Test, Integration and Packaging of MEMS/MOEMS (DTIP)*, pages 1–4, 2015.

[19] A. W. Leissa. *Vibrations of Plates*. National Aeronautics and Space Administration, 1969.

[20] S. Timoshenko and S. Woinowsky-Kreiger. *Theory of Plates and Shells*. McGraw-Hill Higher Education, New York, 1964.

[21] M. Krenkel, M. Kircher, M. Kupnik, and S. G. Koch. CMUT with mechanically coupled plate actuators. In *19th International Conference on Thermal, Mechanical and Multi-Physics Simulation and Experiments in Microelectronics and Microsystems*, 2018.

[22] A. Lohfink and P.-C. Eccardt. Linear and nonlinear equivalent circuit modeling of CMUTs. *IEEE Transactions on Ultrasonics, Ferroelectrics and Frequency Control*, 52(12):2163–2172, 2005.

[23] D. T. Blackstock. *Fundamentals of physical acoustics*. John Wiley & Sons, Inc., 2000.

[24] K. Magnus, K. Popp, and W. Sextro. *Schwingungen*. Springer Vieweg, Wiesbaden, 2016.

[25] I. O. Wygant, M. Kupnik, and B. T. Khuri-Yakub. Analytically Calculating Membrane Displacement and the Equivalent Circuit Model of a Circular CMUT Cell.

In *IEEE International Ultrasonics Symposium*, pages 2111–2114. 2008.

[26] S. D. Senturia. *Microsystem Design*. Springer Science + Business Media New York, 2001.

[27] M. Klemm. *Acoustic Simulation and Characterization of Capacitive Micromachined Ultrasonic Transducers*. PhD thesis, TU Dresden, 2017. ISBN: 978-3-95908-100-9.

[28] V. Walter, G. Bourbon, and P. Le Moal. Residual stress in capacitive micromachined ultrasonic transducers fabricated with anodic bonding using soi wafer. In Giorgio Sberveglieri and Vittorio Ferrari, editors, *Eurosensors, European Conference on Solid-State Transducers*, volume 87, pages 883–886. 2014.

[29] W. P. Mason. *Electromechanical Transducers and Wave Filters*. D. Van Nostrand Company, Inc., Toronto, New York, London, 1948.